Journal of Nuclear Medicine, published on November 18, 2021 as doi:10.2967/jnumed.121.262925

Towards a patient-specific traceable quantification of SPECT/CT-based radiopharmaceutical distributions.

Authors:

Anna-Lena Theisen

Prof. Dr. Michael Lassmann

Dr. Johannes Tran-Gia*

Affiliation:

Department of Nuclear Medicine

University of Würzburg

Oberdürrbacher Str. 6

97080 Würzburg, Germany

***Corresponding Author**

Phone: +49-931-201-35421

Email: Tran_J@ukw.de

Running Title:

Towards inhomogeneous patient-specific kidney phantoms

ABSTRACT

Quantitative SPECT/CT imaging is currently the state-of-the-art for peri-therapeutic monitoring of radiopharmaceutical distributions. Due to poor resolution, however, the verification of SPECT/CT-based activity distributions is of particular importance. Due to the lack of a ground truth in patient measurements, phantoms are commonly used as a substitute for clinical validation of quantitative SPECT/CT. Due to the time-consuming and erroneous preparation of multi-compartment phantoms, e.g. for the kidney, the usually very complex internal activity distributions are typically replaced by one- or two-compartment models. To provide a simplified solution for generating inhomogeneous activity distributions, this work presents a methodology for designing single-compartment phantoms that mimic inhomogeneous spatial activity distributions by internal filling structures of different volume fractions.

Methods: A series of phantoms with different filling structures was designed, 3D printed, and measured. After assessing the feasibility of the presented approach in a simple geometry, a set of three patient-specific kidney phantoms was designed based on the contrast-enhanced CT of a patient suffering from metastatic castration-resistant prostate cancer. Internal gyroid structures of different wall thickness were used in renal medulla and cortex to reproduce the inhomogeneous activity distribution observed in a peri-therapeutic SPECT/CT

acquisition 24-hours post [^{177}Lu]Lu-PSMA injection (apparent activity concentration ratios of 1:1, 1:3.5, and 1:7.5). After 3D printing, SPECT/CT experiments were performed and the results were compared to the patient data for different reconstruction settings (iterations, subsets, and post-filtering).

Results: A good agreement was found between phantom designs and fabricated phantoms (based on high-resolution CT). No internal filling structures were visible in any of the SPECT images, indicating a sufficiently small feature size. While a good visual and quantitative agreement was achieved for certain combinations of filling structure and reconstruction, a histogram analysis indicated an even more complex activity distribution in the patient than represented by the two compartments assumed in our model.

Conclusion: The proposed methodology provides patient-specific phantoms mimicking inhomogeneous activity distributions while using a single stock solution, thus simplifying the filling process and reducing uncertainties in the activity determination. This enables an unprecedented possibility for patient-specific evaluation of radiopharmaceutical uptake, reducing uncertainties in internal dosimetry and individualized treatments.

INTRODUCTION

A fundamental problem in the clinical validation of new imaging technology such as quantitative imaging of radiopharmaceutical distributions, is the lack of a ground truth in patient measurements. Since nuclear medicine imaging procedures are typically non-invasive, direct validation of the measured radiopharmaceutical distribution on the basis of tissue samples is only possible in the rarest of cases. As an example, de Jong et al. revealed the radioactivity distribution in the normal human kidney after intravenous injection of [^{111}In-diethylenetriaminepentaacetic acid (DTPA)]octreotide using SPECT scanning before and ex vivo autoradiography of the kidney after nephrectomy in three men with single primary renal tumors (*1*). In most cases for which such information is not available, however, imaging methodologies can only be validated non-patient-specifically based on anthropomorphic phantom measurements.

Industrially produced phantoms, which are widely used for commissioning and quality control in nuclear medicine imaging, typically consist of one or more fillable compartments of simple geometries (e.g., spheres or cylinders). Inhomogeneous activity distributions are typically achieved by assembling a set of single-compartment phantom inserts separately filled with radioactive stock solutions of different activity concentrations. This, however, increases the complexity and thus the error susceptibility of the phantom preparation, as each

separately filled compartment adds to the total uncertainty of the measurement (e.g., due to errors in activity and filling volume of each stock solution). On the way towards more patient-specific phantoms, increasingly complex 3D-printed phantoms have recently been proposed for quality assessment of SPECT/CT quantification (*2*-*5*). The combination of low costs, yet very flexible design options, makes the technology an ideal supplement for or even alternative to industrially produced phantoms. While in the first implementations of 3D printing technology for nuclear medicine phantom production, simple geometries with a single fillable compartment were implemented (*3*), these designs were quickly replaced by more complex structures consisting of multiple (mostly two) separately fillable compartments (*4*,*5*). Despite many advancements in the field of 3D printing for nuclear medicine phantom production, inhomogeneous activity distributions within a single compartment have not yet been achieved, leaving the issue of patient-specific assessment of SPECT/CT imaging unresolved.

In this work, we present a way of achieving spatially inhomogeneous activity distributions in a single fillable compartment by internal filling structures of different volume fractions. This leads to apparently inhomogeneous activity distributions in SPECT/CT imaging if the structure size is smaller than the SPECT resolution, while keeping phantom filling as simple as possible. The methodology was first developed and tested in a simple cuboid geometry for

validation, and was then applied to create a patient-specific multi-compartment kidney of a patient suffering from metastatic castration-resistant prostate cancer that had previously undergone [^{177}Lu]Lu-PSMA therapy at our institution.

METHODS

SPECT/CT imaging

All SPECT/CT data in this work (phantom as well as patient data) were acquired with a Siemens Intevo Bold SPECT/CT system with 9.5-mm crystal thickness, medium energy low-penetration collimator, 180° configuration, automatic contouring, continuous mode, 60 views, 10 s per view, 256 × 256 matrix, and 3 energy windows (20% around the main photopeak of 208 keV with 2 adjacent 10% windows). Subsequent to the SPECT acquisition, low-dose CT imaging is performed for attenuation correction (130 kVp, 512 × 512 pixels, 1.0 × 1.0 × 3.0 mm resolution). Reconstructions were performed using xSPECT Quant, automatically converting counts to activity concentration based on a NIST-traceable cross-calibration (the calibration of this quantitative reconstruction is performed regularly as recommended by the manufacturer) using 1 subset with different combinations of iterations (12 / 24 / 48) and post-filters (0 mm / 10 mm / 20 mm). All activities were decay-corrected to the starting time of the SPECT/CT acquisition.

The patient whose data were used for this study signed a written informed consent and the local ethics committee expressed no objections to the retrospective evaluation and publication of the data in accordance with data protection regulations (reference number 20200915 01).

Gyroid Structure

The basic idea is to achieve an apparently inhomogeneous signal distribution in SPECT phantoms by using a phantom filled with a radioactive solution of homogeneous activity concentration in combination with a filling structure of spatially varying volume fraction (fraction of volume occupied by the structure). As the structure fills space and thereby displaces radioactive solution to varying extents in different areas of the phantom, the apparent activity distribution (e.g., for SPECT voxels which are typically in the range between 2 and 5 mm edge length) can be varied by changing the volume fraction of the filling structure. The mass density of the hardened photopolymer resin is (1.22 ± 0.01) g/cm^3, obtained by dividing the caliper-based volume of a 3D-printed solid resin cube of side length (20.00 ± 0.05) mm (measurement of all four edges of a single 3D printed cube) by the weight measured with an ED224S analytical balance (Sartorius AG; average of three measurements). This value lies in the

range of water and soft tissue, ensuring only minor differences in attenuation between the resin and water.

The filling structure needs to be periodic to ensure that i) any excess resin can leave the phantom during the printing process and that ii) radioactive solution can permeate the structure during phantom preparation and emptying. In addition, the range of possible volume fractions should be as large as possible to represent even highly heterogeneous activity distributions. After testing different combinations of cylinders and spheres of different sizes, the gyroid structure (*6*) was selected, as it combines all required properties.

A gyroid (Figure 1) is an infinitely connected triply periodic minimal surface structure without self-intersections. The surface is described by the following equation, where *a* equals the period and *t* affects the thickness of the structure:

$$t\,(x,y,z) = sin\frac{2\pi x}{a}\,cos\frac{2\pi y}{a} + sin\frac{2\pi y}{a}\,cos\frac{2\pi z}{a} + sin\frac{2\pi z}{a}\,cos\frac{2\pi x}{a} \quad [1]$$

Three gyroid representations form the basis for all phantom designs in this work (a fixed period of $a = 4\pi \cdot mm$ was used): Gyroid 1 (G1) had a wall thickness of 0.40 mm, which represents the minimum wall thickness supported by our 3D printer (Form 2, Formlabs). In addition, gyroids of wall thickness 1.29

mm (G2) and 2.65 mm (G3) were used to achieve volume fraction ratios of about 1:3.5 (G2) and 1:7.5 (G3) with regards to G1. These volume fractions were chosen as they cover the range of realistic volume fraction ratios (between 1:1 and 1:8 depending on patient, time after injection, and sub-region of cortex or medulla), which we had previously determined in a retrospective evaluation (*7*) of autoradiography data published by de Jong et al. (*1*).

Cuboid phantom

To validate our assumptions, a phantom was designed by concatenating three cubic structures of dimension $4 \times 4 \times 4$ cm^3, each consisting of one of the three gyroids G1, G2, and G3 (see Figure 2A). After creation in MATLAB R2021a (MathWorks), each of these gyroids was transferred to Netfabb Premium 2021 (Autodesk). In Netfabb, each structure was smoothed (triangle reduction with a maximum average deformation of 0.05 mm) to enable high quality 3D printing. Based on these models, the volume fraction ratios between the different gyroid representations G1, G2, and G3 were determined as follows (intermediate values of the calculation see TABLE 1): First, the volume fraction filled with resin ("resin fraction") was calculated as the quotient of the gyroid structure's volume inside a cube (obtained by Netfabb) and the analytical cube volume. In addition, the fraction of each gyroid volume that was fillable with radioactive

stock solution ("fillable fraction") was calculated as complement of the resin fraction. Lastly, the ratio of these resin fractions with respect to G1 was calculated (resin fraction G2 or G3 divided by resin fraction G1), which will be referred to as "resin fraction ratio". These values are crucial when designing multi-compartment phantoms from two different gyroid representations (e.g., a kidney consisting of cortex and medulla).

To combine the three cubic gyroid structures in a single phantom, a cuboid shell of $4 \times 4 \times 12$ cm^3 inner dimensions and 2 mm wall thickness was designed to enclose the three wall-less gyroid cubes (a top and a bottom part to be agglutinated after placing the gyroids inside, see Figure 2A). This shell included a funnel-shaped filling port. Finally, all parts were combined, and the model was exported in the stereolithography (STL) format.

All preparations for the 3D printing procedure (positioning, slicing, and addition of support structures) were performed in PreForm 3.8.0 (Formlabs), and printing was performed using a Form 2 printer with a layer thickness of 100 µm and the Clear V4 resin (both Formlabs).

Patient-specific kidney phantom

To validate the methodology and demonstrate its potential to assess SPECT-based activity distributions obtained in patients undergoing ^{177}Lu-based

nuclear radiotherapies, we designed a set of patient-specific kidney phantoms, performed ^{177}Lu SPECT/CT acquisitions with these phantoms, and compared the results with a clinical ^{177}Lu SPECT/CT dataset of the same patient (acquired with the same setup and system). The kidney was chosen as it represents one of the most common organs at risk in radionuclide therapies (*8-10*).

The clinical validation was performed based on a peri-therapeutic SPECT/CT dataset of a patient suffering from metastatic castration-resistant prostate cancer who had undergone [^{177}Lu]Lu-PSMA therapy at our institution (acquisition time: 24-hours post-injection). For design of a two-compartment model with different activity concentrations in cortex and medulla, high-resolution and high-contrast morphological data were additionally needed. As the low-dose CT acquired along SPECT/CT scanning is not sufficient to reliably distinguish cortex and medulla, a temporally close contrast-enhanced CT acquisition (Siemens Biograph mCT 64, CT parameters: $0.78 \times 0.78 \times 1.00$ mm^3 resolution, 150 mAs, 100 kVp, pitch factor 0.8, 512x512x866 slices) of the same patient was used. After anonymization (syngo.via, Siemens), the DICOM images were loaded into 3D Slicer 4.10.1 (*11*) for segmentation. First, the contrast-enhanced CT, which provided the anatomical information of cortex and medulla, was registered to the low-dose CT of the peri-therapeutic SPECT/CT acquisition using an affine registration. Then, slice-by-slice segmentations of cortex and

medulla of the left kidney were performed in the registered contrast-enhanced CT. These segmentations were exported in the STL format for further processing (left column of Figure 3A).

To cover a range of different internal activity distributions, a set of three kidney phantoms with different combinations of internal gyroid structures was designed. As the highest uptake is typically expected in the renal cortex, the cortex of all phantoms was filled with gyroid G1, i.e. with the highest fillable fraction available. In contrast, the medulla was filled with a different gyroid representation (G1 to G3) for each phantom, resulting in different resin fraction ratios (1:1, 1:3.55, 1:7.44).

All gyroid compartments were constructed in Netfabb by Boolean operations between the segmentations and the gyroid structures (see Figure 3A). Subsequently, the two gyroid-filled compartments were combined with a kidney shell (wall thickness 1 mm) as well as filling and attachment ports (Figure 3A, center). Finally, the model was exported in the STL format and 3D printed in one piece as described in the previous section (result see Figure 3B).

Refinement of 3D printed phantoms and quality assurance

After printing, all phantoms were refined as follows: To remove excess resin, the phantoms were washed in 99.9% concentrated 2-Propanol (IPA) for

180 min, followed by 60 min of UV post-curing at 60°C to reach the highest possible strength. Afterwards, the support structures were manually removed. Finally, a polyamide M6 plastic thread and a filling funnel (to avoid air bubbles during filling) were glued on with a medium viscosity two-component epoxy adhesive.

For quality assurance, the finished phantoms underwent several quality tests. To check the agreement between the CAD model and the printed phantom, a high resolution CT scan of the phantom was performed using the CT system integrated in our SPECT/CT system (Siemens Intevo Bold, CT parameters: 0.29 × 0.29 × 0.70 mm^3 resolution, 150 mAs, 130 kVp, pitch factor 0.5, 512x512x241 slices) and the CT images were compared to the computer-aided design (CAD) models.

As waterproofness is one of the most important prerequisites for nuclear medicine phantoms, the finished phantoms finally underwent leakage testing. In the same process, the filling volume of each phantom was determined by weighing the phantom before and after filling with a PCB 3500-2 precision mass scale (Kern & Sohn GmbH).

Activity quantification of the patient's kidney

To establish similar measurement conditions between the phantom measurements and the patient measurement, the total activities of the kidney phantom measurements were chosen as similar as possible to the patient kidney. For this purpose, the SPECT/CT-based activity in the left patient kidney 24-hours post-injection was determined by a VOI analysis in the xSPECT Quant reconstructions (i.e., the mean of the activity concentration in a CT-based kidney VOI [Bq/ml], which had been enlarged by 6 mm to account for spill-out, multiplied with the VOI volume [ml] (*12*)). Activity concentrations for the stock solutions to be used in the three kidney phantoms were then calculated by dividing this total activity by the filling volume of each of the kidney phantoms (target activities and activity concentrations along with the actually measured values can be found in TABLE 2 of the Results section).

Quantitative SPECT/CT imaging of the phantoms

To ensure homogeneous solutions and prevent sticking (or plating) of activity to the walls of vessels being used, all stock solutions consisted of ^{177}Lu chloride dissolved in 0.1 M HCl with 100 ppm of stable lutetium (*13*). A VDC-405 radionuclide calibrator with a VIK-202 ionization chamber (Comecer SpA) was used for estimating the activity concentration during the phantom filling

process. Subsequently, accurate activity concentrations were obtained by measuring 1-mL aliquots of all stock solutions (3 per stock solution) in a high-purity germanium detector (HPGe; Canberra GR4020 with GENIE 2000 spectroscopy software) whose energy-dependent efficiency had previously been calibrated with several NIST (National Institute of Standards and Technology)– and NPL (National Physical Laboratory)–traceable standards over the energy range considered. The activity concentrations of the stock solutions were determined by weighing (full minus empty stock solution container) with a PCB 3500-2 precision balance (Kern & Sohn GmbH, readability: 0.01 g, repeatability: 0.02 g). In contrast, the aliquot volumes were weighed in an ED224S analytical balance (Sartorius AG) with a readability of 0.1 mg.

Subsequently, each phantom (cuboid + three kidneys) was filled with a different stock solution (target and measured activity concentrations see TABLE 2). Again, the actual filling volume was determined by weighing (filled minus empty kidney phantom). Last, the phantoms were separately mounted in a water-filled Jaszczak cylinder (Data Spectrum; inside diameter and height are 216 mm and 186 mm, respectively) and SPECT/CT measurements were performed. To make the phantom data as comparable as possible to the patient data, the phantom acquisition was performed with the same acquisition parameters used in the patient acquisition. In contrast, different reconstructions (different Gaussian

post-filters) were applied for phantom and patient data to assess the correspondence between the resulting activity distributions (see section *SPECT/CT imaging*).

Activity concentration–voxel histograms

To semi-quantitatively compare the patient scan to the three patient-specific phantom scans, activity concentration–voxel histograms (the number of voxels containing a measured activity concentration plotted against the respective activity concentration) were calculated in MATLAB based on the SPECT-based distributions of activity concentration by sorting the voxels according to their activity concentration in bins of width 0.01 MBq/ml. Ideally, these histograms should consist of two distributions around the two activity concentrations of the stock solution.

RESULTS

Cuboid phantom

Figure 2 shows the design, fabrication, and validation of the cuboid phantom. Especially the superimposition of the CAD model and the CT image in Figure 2C emphasize the good visual match between model and printed phantom. The SPECT reconstruction in Figure 2D shows apparently different yet homogeneous

activity distributions in each of the three compartments, demonstrating that the dimension of the filling structures is in an adequate range for SPECT/CT imaging with a medium energy collimator.

Figure 4 illustrates the SPECT-based activity distribution inside the gyroid. To avoid resolution effects along the phantom edges, the averages within 2×2 cm^2 square regions-of-interest were calculated in the axial slices and plotted along the axis of the 4×4×12 cm^3 cuboid phantom. In general, the edges are clearly underestimated due to partial volume effects (e.g., between axial positions 0 mm and 8 mm). In contrast, the activity is overestimated in the central area when no or 10 mm post-filtering is applied (solid lines). For the wider 20 mm post-filter, however, the activity is increasingly spilled out of the actual object dimensions (dashed lines), leading to an underestimation of the total activity.

In a quantitative analysis of the cuboid reconstructions (2×2×2 cm^3 VOIs as indicated in Figure 4), the best match between HPGe- and SPECT-based activity was found for reconstructions with a 10-mm Gaussian post-filter (TABLE 3). Here, the nominal activity concentration in each of the gyroids was calculated by multiplying the HPGe-based activity concentration of the stock solution ([0.69 ± 0.01] MBq/ml) with the fillable fraction of the corresponding gyroid (TABLE 1).

Patient-specific kidney phantom

Figure 5 shows design and validation of the three patient-specific two-compartment kidneys. At the bottom of Figure 5, the phantom and the patient CT images were superimposed to emphasize the good match between the outer contours and the internal compartments for all three phantoms. No filling structures were used in the top sections of each phantom to simplify the filling process (green arrows). In addition, the renal pelvis was printed as solid structure to ensure a good printing quality (light blue regions in the CAD models in the center row of Figure 5). The linear attenuation coefficient of our ^{177}Lu SPECT/CT setup was determined as (0.148 ± 0.001) cm^{-1} in a VOI analysis of this solid structure in the associated μ-map.

Figure 6 shows fused SPECT/CT images of the patient (top) and the three phantom acquisitions (bottom). While the 1:1 phantom visually overestimates the activity concentration in the medulla (green arrows), a good visual agreement is obtained for the 1:3.5 phantom. The wide 20-mm filter strongly blurs the image, such that the difference between cortex and medulla signal becomes difficult to assess visually. The 1:3.5 phantom with moderate filtering (10-mm Gaussian) leads to the best visual match.

TABLE 2 shows all activities and the activity concentrations measured with regard to the patient-specific kidney phantom measurements: It shows the

filling volume (i.e., the volume filled with radioactive stock solution), the target activity concentration (based on the SPECT-based activity in the patient kidney), the HPGe-based activity concentration and total kidney activity (activity concentration multiplied with the filling volume) as well as the medulla and cortex activity concentrations (stock solution activity concentration multiplied with fillable fraction of the respective kidney phantom given in TABLE 1), and the SPECT-based total activities (VOI analysis based on the phantom filling volume). All total kidney activities lie within 10% of the SPECT-based total kidney activity of 94.9 MBq and thus close enough to provide equivalent measurement conditions. As the resolution lies in the range of the medulla size, considerable spill-out and spill-in is to be expected between the cortex and the medulla. In consequence, a separate evaluation of both compartments based on the SPECT is extremely prone to errors and was not performed.

SPECT-based activity concentration–voxel histograms (creation see section *Activity concentration–voxel Histograms*) are given in Figure 7. While the patient data are plotted in black, each phantom is indicated by a different color (red: 1:7.5, blue: 1:3.5, green: 1:1). The curves depict the number of voxels (vertical axis) containing a certain activity concentration (horizontal axis, bin size 0.01 MBq/ml), vertical dashed lines indicate the theoretical (HPGe-based) activity concentrations in medulla and cortex (the values are given in TABLE 2).

Ideally, the histogram should consist of activity distributions around these dashed lines. For the 1:1 phantom, there is only a single vertical green line as both compartments have the same filling structure and, therefore, activity concentration. As expected, the post-filters smoothen higher activity concentration peaks, resulting in a shift towards lower activity concentrations in the filtered histograms (e.g., Figure 7C). For the 1:7.5 resin fraction ratio (red), the peaks of the unfiltered as well as the 10-mm Gaussian curves lie in the range defined by the two theoretical activity concentrations, while the 20-mm Gaussian filter leads to an underestimation. For the 1:3.5 resin fraction ratio (blue), the 10-mm Gaussian filter leads to an activity concentration peak between the two theoretical values. In contrast, no filtering or a 20-mm Gaussian filter result in an over- or underestimation of the theoretical activity concentrations, respectively. For the 1:1 resin fraction ratio (green), a good quantitative agreement is found for the 10-mm post-filter, with the SPECT-based activity concentration peak centered exactly on the HPGe-based activity concentration. While the 20-mm Gaussian filter leads to the previously described underestimation, not applying any filter leads to a wide spectrum of activity concentrations (e.g., a maximum activity concentration up to two times higher than the theoretical value). In contrast to the colored phantom curves, which all exhibit a maximum, all patient curves (black) are monotonically decreasing.

DISCUSSION

One of the main problems in the clinical validation of quantitative SPECT/CT is the lack of a ground truth in patient measurements. Depending on the image reconstruction applied, a wide variety of different spatial activity distributions can be generated without knowledge about the ground truth (*7*), as can be seen in Figure 7 (black lines). This observation demonstrates that an assessment of the activity distribution on a voxel level, based purely on SPECT/CT imaging, is problematic (*7*) and that, for validation, additional methods such as the measurement of realistic, ideally patient-specific phantoms, should ideally complement the image quantification process. Up to now, the complexity of phantom measurements has been restricted by the availability of phantoms. Multi-compartment phantoms usually consisted of separate compartments filled with radioactive stock solutions of different activity concentrations, thus considerably increasing the sources of uncertainty. As a major advancement, the approach proposed in this work achieves to mimic inhomogeneous activity distributions in SPECT/CT with only a single fillable compartment by making use of internal gyroid structures of different volume fractions, considerably simplifying phantom preparation and reducing uncertainties.

In addition, the new method represents another important advancement: While it was previously impossible to achieve continuous transitions of activity concentrations, this changes by the introduction of filling structures of different volume fractions. If further developed, multiple thin gyroid layers of different wall thickness could be placed adjacent to each other to achieve continuously varying apparent activity concentrations, while still requiring only a single stock solution. This could take the individualization of phantoms to an unprecedented new level.

In comparison to standard, single-compartment phantoms, the gyroid structure features a large surface area with many very small congruent channels. This leads to an increased occurrence of surface tension–related air bubbles in these regions, resulting in small black regions in the CT (blue arrows in Figure 6). This can, however, be considerably improved by reducing the surface tension of the stock solution, e.g. by adding soapy water. Through the addition of soap in our stock solutions, only few air bubbles remained in the phantoms imaged in this work (e.g., Figure 6).

Another subject to be discussed is the printing process. To keep the wall thickness as small as possible (e.g., 0.4 mm thickness of the renal cortex gyroid structure), we applied a stereolithography based 3D printing technique which is based on a photopolymer resin that is hardened layer-by-layer using an ultraviolet

laser beam. The relatively large maximum unsupported overhang length of 3 mm allowed the entire kidney phantom to be printed as one part, in contrast to the previously used fused deposition modeling technique, where the phantoms had to be printed in several individual parts (*3,5,7*). However, the techniques require excess, uncured resin to escape the gyroid structure, which can be problematic for gyroids of large wall thickness due to the low viscosity of the resin. For our Form 2 printer, our standard period of $4\pi \cdot mm$ with a wall thickness between 0.40 mm and 2.65 mm resulted in a realistic range of activity concentration ratios between renal medulla and cortex (between 1:1 and 1:8 (*1,7*)). Provided careful modeling and positioning of the CAD models prior to 3D printing, reliable printing was possible even for the largest wall thickness of 2.65 mm.

For validation, the model was tested using a patient-specific two-compartment kidney model. A direct quantitative comparison between phantom and patient images with conventional means (e.g. using measures such as the structural similarity index, SSIM) is almost impossible due to the isolated nature of the phantom in comparison to the patient kidney that is surrounded by anatomical structures. To perform at least a semi-quantitative evaluation, a histogram analysis (Figure 7) was applied to illustrate the differences. As an in-depth analysis of the difference between activity distributions and absorbed dose distributions for ^{177}Lu has demonstrated virtually no differences in their spatial

distributions in a previous study (*7*), we only considered the activity concentration in this work.

Due to the unevenly shaped interface between cortex and medulla in combination with the SPECT resolution, which is unable to resolve the gyroid channels, the two theoretical peaks (vertical dashed lines) merge into a single peak in the SPECT/CT-based distribution of activity concentrations (Figure 7). In contrast, all patient curves (black lines) are monotonically decreasing, indicating that the underlying activity distribution in the patient kidney is more heterogeneous than the distribution modeled by the two compartments in this study.

Given the numerous potential differences between any patient and phantom measurement (e.g., different scatter environments, different contouring of the camera, potential background radiation in the patient, patient motion) affecting SPECT/CT-based quantification, some discrepancy between patient and associated phantom measurements is always to be expected. Considering this, the degree of similarity between patient and phantom (Figure 6, center column) can be considered as close to the maximum achievable. For this reason, we only provide an analysis of three example post-filters instead of trying to find the best combination of iterations, subsets, and post-filter.

The routine application of dosimetry to optimize the efficacy of radionuclide therapies, and thus the need for a routine patient-specific validation of quantitative SPECT/CT imaging, currently still seems to be some way ahead. If internal individualized dosimetry becomes established, however, the methodology presented here could form the basis for a patient-specific optimization of quantitative SPECT/CT imaging (e.g., regarding imaging and reconstruction parameters). Provided a certain quality level of SPECT/CT-based dose-voxel histograms, such quantitative measures could form a cornerstone for planning and monitoring of individualized radionuclide therapies, as it is already standard in external beam radiotherapy.

CONCLUSION

In summary, we have shown that the use of internal support structures allows phantom measurements of inhomogeneous activity distributions using only a single stock solution of a single activity concentration. By keeping the dimensions of the filling structures well below the resolution of the imaging system, we were able to mimic the internal activity distribution in the kidney of a patient treated with ^{177}Lu-PSMA (24 hours post injection SPECT/CT). In a quantitative analysis, however, it was shown that a representation of the kidney by only two compartments (renal cortex and medulla) of different apparent activity concentrations still represents an oversimplification. For an even better representation, more different compartments would be required.

DISCLOSURE

M. Lassmann has received research grants by IPSEN Pharma and Nordic Nanovector.

FUNDING

This study was funded by a grant of the German Research Foundation (Deutsche Forschungsgemeinschaft TR 1380/1-1). The funders had no role in the design of the study; in the collection, analyses, or interpretation of data; in the writing of the manuscript, or in the decision to publish the results.

KEY POINTS

Question: Is it possible to design patient-specific kidney phantoms with only a single fillable compartment yet an inhomogeneous activity distribution for assessment of SPECT/CT-based peri-therapeutic monitoring of radiopharmaceutical distributions?

Pertinent Findings: Using the presented methodology, we achieved to produce a patient-specific kidney phantom for a patient suffering from metastatic castration-resistant prostate cancer, visually and quantitatively mimicking a peri-therapeutic SPECT/CT acquisition 24-hours post-injection of [^{177}Lu]Lu-PSMA. Despite the restriction to only a single compartment for ease of phantom preparation, an inhomogeneous activity distribution in the patient SPECT/CT could be reproduced.

Implication for Patient Care: The presented methodology enables a patient-specific assessment of activity distributions and thus absorbed dose depositions in organs at risk in radionuclide therapy.

REFERENCES

1. De Jong M, Valkema R, Van Gameren A, et al. Inhomogeneous localization of radioactivity in the human kidney after injection of [^{111}In-DTPA]octreotide. *J Nucl Med.* 2004;45:1168-1171.

2. Gear JI, Long C, Rushforth D, Chittenden SJ, Cummings C, Flux GD. Development of patient-specific molecular imaging phantoms using a 3D printer. *Med Phys.* 2014;41:082502.

3. Tran-Gia J, Schlögl S, Lassmann M. Design and fabrication of kidney phantoms for internal radiation dosimetry using 3D printing technology. *J Nucl Med.* 2016;57:1998-2005.

4. Robinson AP, Tipping J, Cullen DM, et al. Organ-specific SPECT activity calibration using 3D printed phantoms for molecular radiotherapy dosimetry. *EJNMMI Phys.* 2016;3:12.

5. Tran-Gia J, Lassmann M. Optimizing image quantification for ^{177}Lu SPECT/CT based on a 3D printed 2-compartment kidney phantom. *J Nucl Med.* 2018;59:616-624.

6. Schoen AH. *Infinite periodic minimal surfaces without self-intersections (NASA technical note, NASA TN D-5541).* Washington: National Aeronautics and Space Administration; 1970.

7. Tran-Gia J, Salas-Ramirez M, Lassmann M. What you see is not what you get – on the accuracy of voxel-based dosimetry in molecular radiotherapy. *J Nucl Med.* 2019;61:1178-1186.

8. Kwekkeboom DJ, de Herder Ww Fau - Kam BL, Kam Bl Fau - van Eijck CH, et al. Treatment with the radiolabeled somatostatin analog [^{177}Lu-DOTA 0,Tyr3]octreotate: toxicity, efficacy, and survival. *J Clin Oncol.* 2008;26:2124-2130.

9. Bodei L, Cremonesi M, Ferrari M, et al. Long-term evaluation of renal toxicity after peptide receptor radionuclide therapy with ^{90}Y-DOTATOC and ^{177}Lu-DOTATATE: the role of associated risk factors. *Eur J Nucl Med Mol Imaging.* 2008;35:1847-1856.

10. Vegt E, De Jong M, Wetzels JF, et al. Renal toxicity of radiolabeled peptides and antibody fragments: mechanisms, impact on radionuclide therapy, and strategies for prevention. *J Nucl Med.* 2010;51:1049-1058.

11. Fedorov A, Beichel R, Kalpathy-Cramer J, et al. 3D Slicer as an image computing platform for the quantitative imaging network. *Magn Reson Imaging.* 2012;30:1323-1341.

12. Tran-Gia J, Lassmann M. Characterization of noise and resolution for quantitative ^{177}Lu SPECT/CT with xSPECT Quant. *J Nucl Med.* 2019;60:50-59.

13. Tran-Gia J, Denis-Bacelar AM, Ferreira KM, et al. A Multi-Centre and Multi-National Evaluation of the Accuracy of Quantitative Lu-177 SPECT/CT Imaging Performed Within the MRTDosimetry Project. *EJNMMI Phys.* 2021.

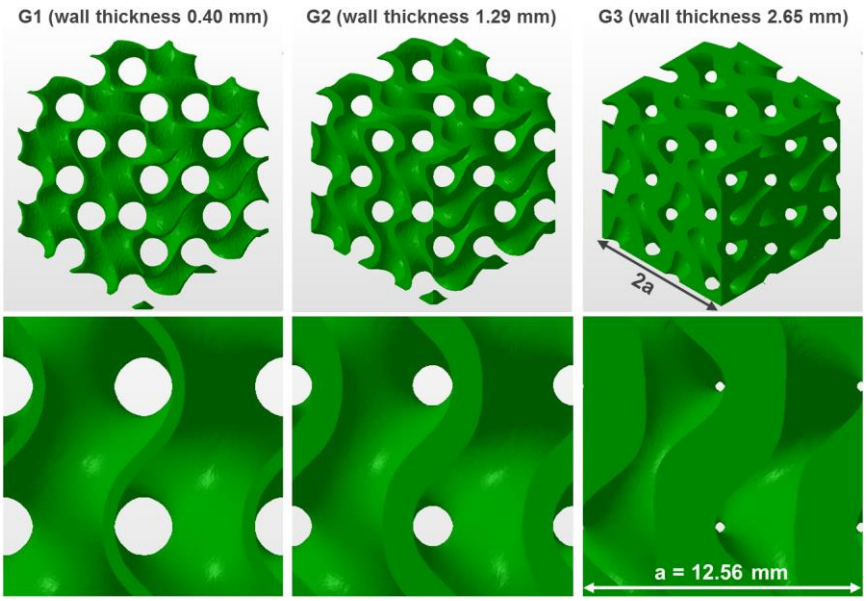

Figure 1: Gyroid structures used in this work. Top: Gyroid cubes (edge length 2*a*) for a period of a = 12.56 mm and different wall thicknesses (G1: 0.40 mm, G2: 1.29 mm, G3: 2.65 mm). Bottom: Corresponding cross-sections (only a single period is depicted) to illustrate the gyroid features (period, wall thickness) and the spatial volume filled by the gyroid.

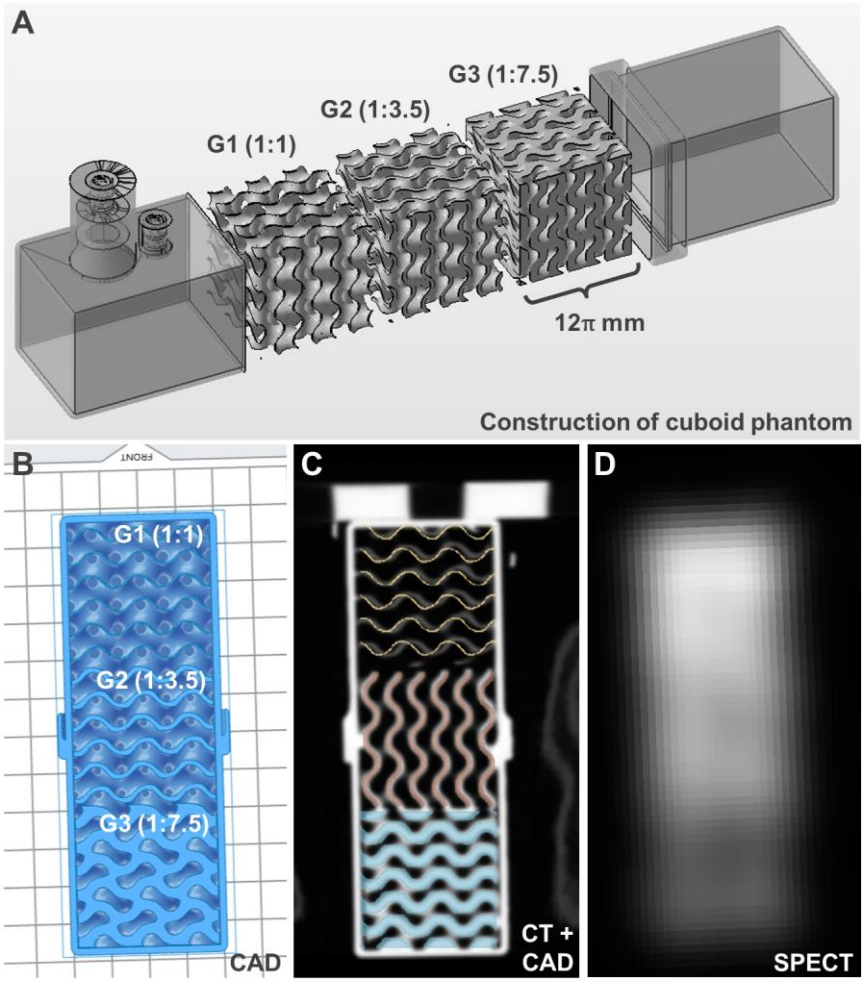

Figure 2: Cuboid phantom. A: Model components (three gyroid cubes of different volume fraction ratio and a shell consisting of two parts). B: Cross-section through CAD model. C: Cross-section through CT (gray scale) superimposed by the CAD model (different colors). D: Cross-section of the SPECT reconstruction (48 iterations, 1 subset, and 10 mm post-filter).

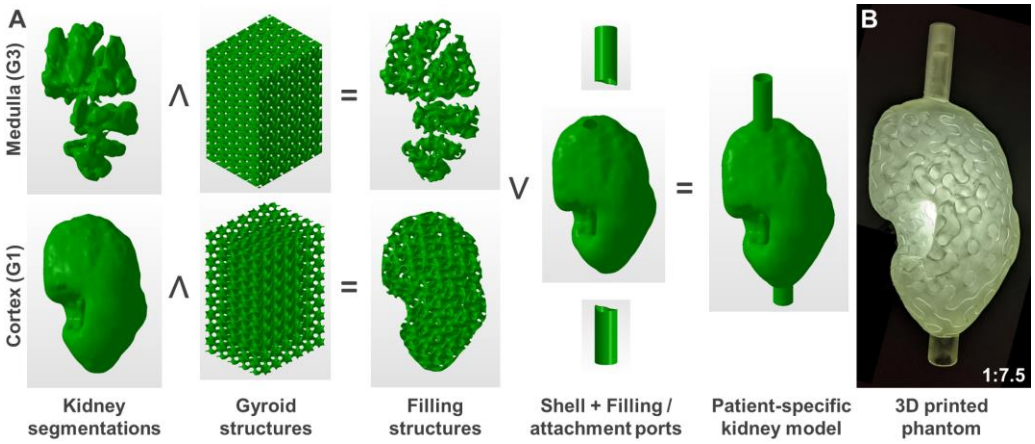

Figure 3: Design of a patient-specific two-compartment kidney phantom. A: Boolean operations necessary to generate a kidney CAD model out of patient-specific kidney VOIs, different gyroid structures (example: G1 and G3 for cortex and medulla, respectively), attachment and filling ports, and a patient-specific kidney shell (∧: Boolean "and", ∨: Boolean "or"). B: 3D printed 1:7.5 kidney phantom.

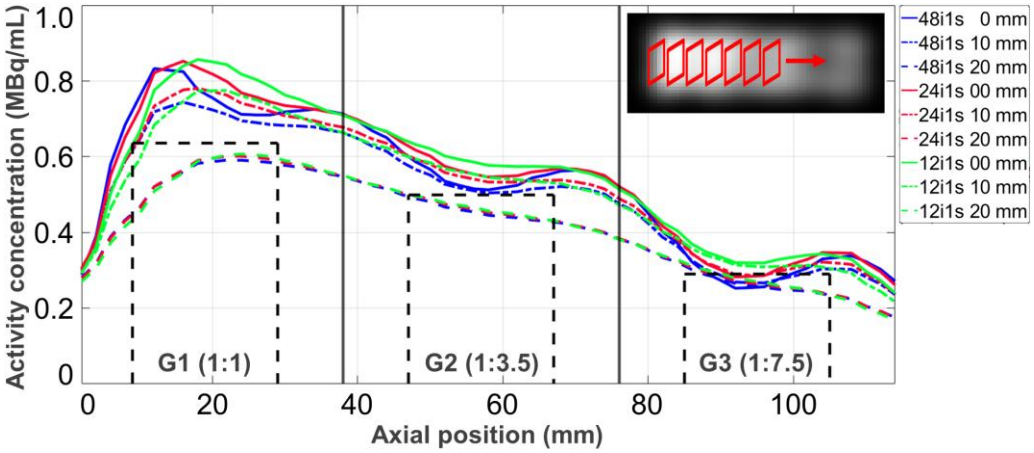

Figure 4: Quantitative analysis of the cuboid. Depicted is the mean activity concentration in square regions-of-interest plotted in axial direction for different reconstruction parameters (number of iterations and post-filters). The positioning of the axial regions-of-interest is illustrated in the top right by red boxes in the SPECT reconstruction. The solid black vertical lines represent the borders between the different gyroid cubes. The dashed black rectangles indicate the axial position of the 2×2×2 cm^3 cubes used for the quantitative analysis (height of each box: HPGe-based activity concentration).

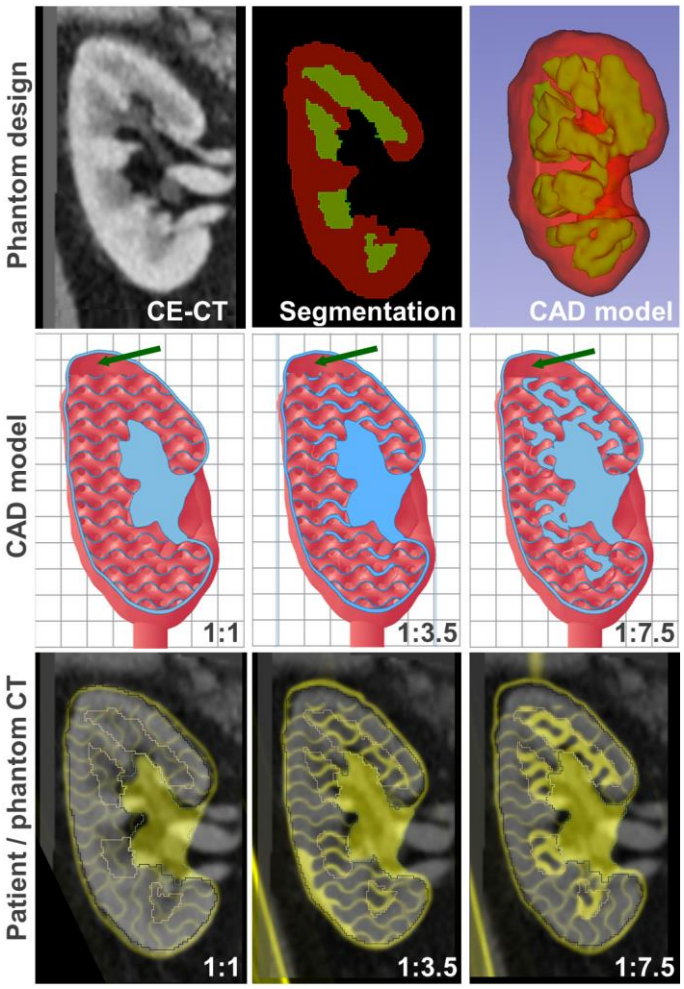

Figure 5: Design and validation of patient-specific kidney phantoms. Top (left to right): Coronal contrast-enhanced (CE) CT slice of the patient kidney. Segmented cortex (red) and medulla (green). 3D model of the segmentation. Center: Cross-sections through CAD models (green arrows: top sections without internal structure) for all three phantom designs (grid dimension: 1 cm). Bottom: Contrast-enhanced patient CT (gray scale) overlaid with the CT of the phantom kidney (yellow) for all three phantom designs.

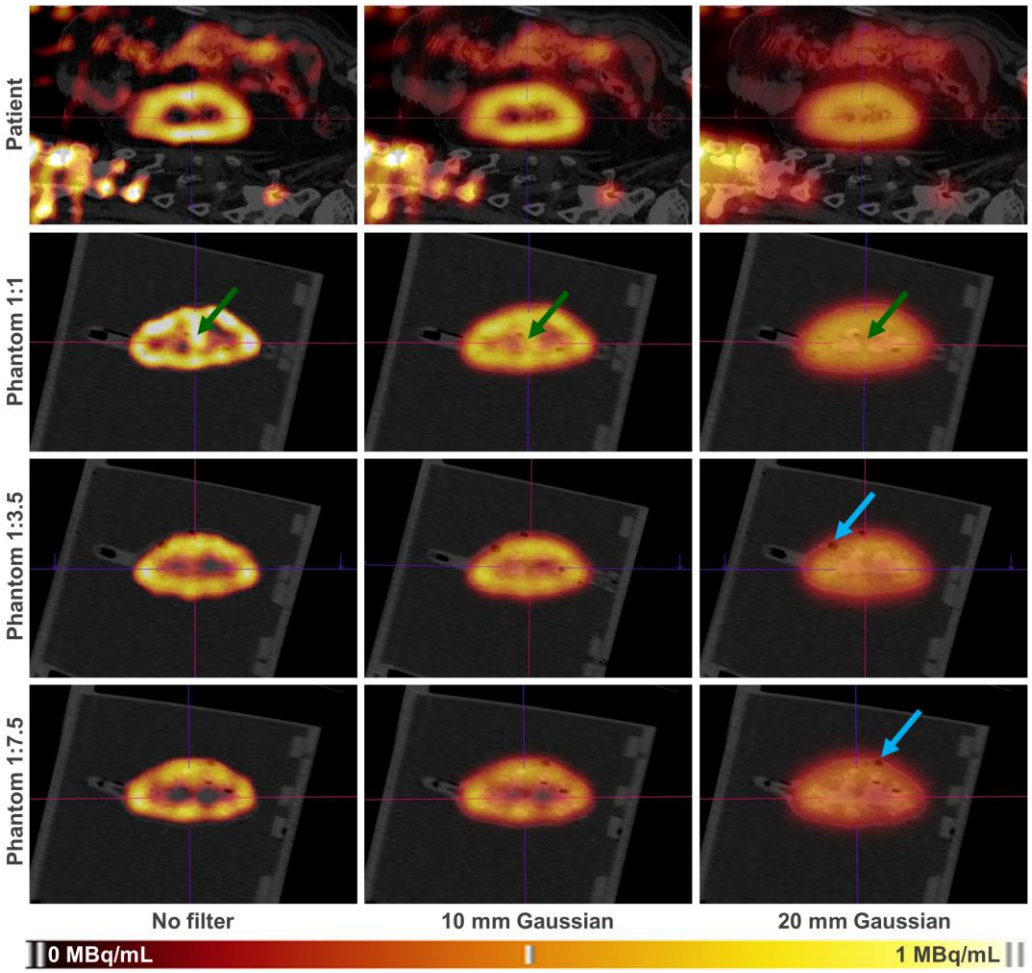

Figure 6: SPECT/CT fusions of the patient acquisition (top row) and the three phantoms (resin fraction ratios of 1:1, 1:3.5, and 1:7.5) for different post-filters (left to right: 0 mm / 10 mm / 20 mm). Green arrows: overestimation of the activity concentration in the medulla for resin fraction ratio 1:1. Blue arrows: surface tension–related air bubbles.

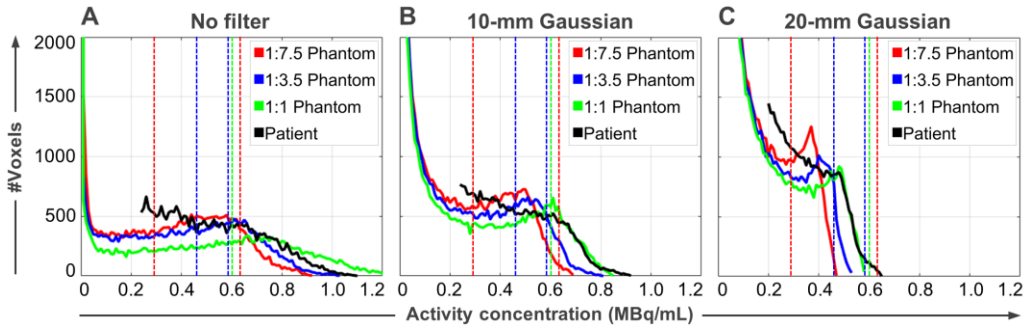

Figure 7: Activity concentration–voxel histograms for the patient (black) and the three phantoms (red: 1:7.5, blue: 1:3.5, green: 1:1) for 48 iterations, 1 subset and different Gaussian post-filters of 0 mm (A), 10 mm (B), and 20 mm (C) full width at half maximum. While the solid curves depict the number of voxels containing a certain activity concentration, the vertical dashed lines indicate the HPGe-based activity concentrations in medulla and cortex (values see TABLE 2).

TABLE 1

Calculation of the resin fraction and fillable fraction for the three cuboid structures. In addition, the resin fraction ratio of G2 and G3 with respect to G1 are given.

Gyroid	Wall thickness (mm)	Resin fraction	Fillable fraction	Resin fraction ratio
G1	0.40	0.078	0.922	(1:1)
G2	1.29	0.277	0.723	1:3.55
G3	2.65	0.580	0.420	1:7.44

TABLE 2

Activities and the activity concentrations measured with regard to the patient-specific kidney phantom measurements. Filling volume (V) as well as target, HPGe-based and SPECT-based activity concentrations (c) and total kidney activities (A). The medulla and cortex concentrations were calculated based on the fillable fractions (TABLE 1). The SPECT-based target total activity for the patient kidney was 94.9 MBq.

		Target	HPGe-based				SPECT-based		
Ratio	V (ml)	c (MBq/ml)	c (MBq/ml)	A (MBq)	$c_{Medulla}$ (MBq/ml)	c_{Cortex} (MBq/ml)	A_{0mm} (MBq)	A_{10mm} (MBq)	A_{20mm} (MBq)
1:1	149.8	0.63	0.65	97.4	0.60	0.60	103.8	103.7	103.6
1:3.5	140.2	0.67	0.63	88.3	0.46	0.58	93.6	93.5	93.5
1:7.5	131.5	0.72	0.68	89.4	0.29	0.63	87.8	87.7	87.7

TABLE 3

Quantitative evaluation of different gyroid structures inside the cuboid phantom (vertically: different numbers of iterations, horizontally: post-filters of different full widths at half maximum). All activity concentrations are given in MBq/mL.

Iterations	No post-filter	10-mm Gaussian	20-mm Gaussian
Activity concentration G1 (1:1) gyroid (HPGe-based): 0.64			
12	0.81	0.74	0.58
24	0.79	0.74	0.58
48	0.76	0.71	0.57
Activity concentration G2 (1:3.5) gyroid (HPGe-based): 0.50			
12	0.59	0.55	0.46
24	0.57	0.55	0.46
48	0.54	0.52	0.45
Activity concentration G3 (1:7.5) gyroid (HPGe-based): 0.29			
12	0.33	0.31	0.26
24	0.32	0.31	0.26
48	0.29	0.29	0.25

GRAPHICAL ABSTRACT